UNCLASSIFIED

AD-A169 240

REPORT DOCUMENTATION PAGE

1a REPORT SECURITY CLASSIFICATION Unclassified		1b RESTRICTIVE MARKINGS		
2a SECURITY CLASSIFICATION AUTHORITY N/A		3 DISTRIBUTION/AVAILABILITY OF REPORT Approved for public release; distribution is unlimited.		
2b DECLASSIFICATION/DOWNGRADING SCHEDULE N/A				
4 PERFORMING ORGANIZATION REPORT NUMBER(S) AFATL-TR-86-52		5 MONITORING ORGANIZATION REPORT NUMBER(S)		
6a NAME OF PERFORMING ORGANIZATION Air Force Armament Laboratory Aerodynamics Branch	6b OFFICE SYMBOL (If applicable) AFATL/FXA	7a NAME OF MONITORING ORGANIZATION Air Force Armament Laboratory Aerodynamics Branch		
6c ADDRESS (City, State, and ZIP Code) Eglin AFB, FL 32542-5434		7b ADDRESS (City, State, and ZIP Code) Eglin AFB, FL 32542-5434		
8a NAME OF FUNDING/SPONSORING ORGANIZATION N/A	8b OFFICE SYMBOL (If applicable) N/A	9 PROCUREMENT INSTRUMENT IDENTIFICATION NUMBER N/A		
8c ADDRESS (City, State, and ZIP Code) N/A		10 SOURCE OF FUNDING NUMBERS		

8c ADDRESS (City, State, and ZIP Code)	PROGRAM ELEMENT NO 61601F	PROJECT NO 2567	TASK NO 03	WORK UNIT ACCESSION NO 08

11 TITLE (Include Security Classification)

An Analysis of Elliptic Grid Generation Techniques Using an Implicit Euler Solver.

12 PERSONAL AUTHOR(S)
Jon S. Mounts, Agusto Martinez, and Joe F. Thompson

13a TYPE OF REPORT Interim	13b TIME COVERED FROM Oct 85 TO Sep 86	14 DATE OF REPORT (Year, Month, Day) 86-06-09	15 PAGE COUNT 13

16 SUPPLEMENTARY NOTATION
None

17	COSATI CODES		18 SUBJECT TERMS (Continue on reverse if necessary and identify by block number)
FIELD 01	GROUP 01	SUB-GROUP	Grid Generation Computational Aerodynamics

19 ABSTRACT (Continue on reverse if necessary and identify by block number)
Several control function interpolation techniques in a general three-dimensional elliptic grid generation code and their effects on flow solutions using an implicit Euler algorithm are examined. These results will serve to guide the design of control function procedures and interpolation techniques in general grid generation codes. Three configurations and three grid types ("O", "C", and "H" grids) are examined. The results indicate that the selection of the control function interpolation techniques, which affect grid spacing, should be based on boundary curvature and spacing. The selection of the interpolation technique can then be made transparent to the user of general grid generation codes.

DTIC
SELECTE
JUN 27 1986

S

20 DISTRIBUTION/AVAILABILITY OF ABSTRACT ☒ UNCLASSIFIED/UNLIMITED ☐ SAME AS RPT ☐ DTIC USERS	21 ABSTRACT SECURITY CLASSIFICATION Unclassified	
22a NAME OF RESPONSIBLE INDIVIDUAL JON S. MOUNTS	22b TELEPHONE (Include Area Code) (904) 882-3124	22c OFFICE SYMBOL FXA

DD FORM 1473, 84 MAR

83 APR edition may be used until exhausted
All other editions are obsolete

AN ANALYSIS OF ELLIPTIC GRID GENERATION TECHNIQUES
USING AN IMPLICIT EULER SOLVER

Jon S. Mounts[*]
Agusto Martinez[*]
U.S. Air Force Armament Laboratory
Eglin Air Force Base, Florida

Joe F. Thompson[+]
Mississippi State University
Mississippi State, Mississippi

Abstract

Several control function interpolation techniques in a general three-dimensional elliptic grid generation code and their effects on flow solutions using an implicit Euler algorithm are examined. These results will serve to guide the design of control function procedures and interpolation techniques in general grid generation codes. Three configurations and three grid types ("O", "C", and "H" grids) are examined. The results indicate that the selection of the control function interpolation techniques, which affects grid spacing, should be based on boundary curvature and spacing. The selection of the interpolation technique can then be made transparent to the user of general grid generation codes.

Nomenclature

g_{mn}	-	elements of covariant metric tensor (m = 1,2,3; n = 1,2,3)
g^{mn}	-	elements of contravariant metric tensor (m = 1,2,3; n = 1,2,3)
r	-	Cartesian position vector ($r = xi + yj + zk$)
x,y,z	-	three Cartesian coordinates
ξ^i	-	three curvilinear coordinates (i = 1,2,3) of transformed region
P_n	-	"Control functions" which serve to control spacing and orientation of grid lines (n = 1,2,3)
r	-	local radius of curvature
D	-	diameter
M_∞	-	freestream Mach number
α	-	angle of attack (degrees)
C_p	-	pressure coefficient
C_p^*	-	sonic pressure coefficient

Introduction

In the field of computational fluid dynamics (CFD), current research is aimed primarily at improving both the accuracy and efficiency of the numerical techniques employed in solving fluid flow, heat transfer, and combustion problems.[1] Improvements must be made in both of these areas if CFD is to become a viable partner to the wind tunnel in aerodynamic design. Numerical grid generation requires technology development and has been cited as a major pacing item for realistic aircraft/missile applications.[2] The techniques of

numerical grid generation, and its application in the numerical solution of partial differential equations, are covered in detail in a recent text on the subject.[3] Several surveys of the field have also been given,[4-7] and three conference proceedings dedicated to this area have been published.[8-10]

The computational grid, or mesh, working in conjunction with the flow solver can have a substantial impact on the aerodynamic solution;[11] therefore, it is the objective of this analysis to examine several gridding procedures and their effects on Euler approximations. This study was conducted as part of the development effort of a general three-dimensional grid code for realistic aircraft/missile configurations. The purpose of this analysis is to demonstrate the viability of automatic determination of the control function, in the elliptic grid generation system, from the boundary point distributions using separate interpolation techniques for the terms arising from spacing and local curvature. These results will serve to guide the design of control function procedures and interpolation techniques to be made automatic and transparent to the user in this code and are similarly of relevance to the design of general grid generation codes by others.

Grid-Generation

A general three-dimensional grid generation code has been written which allows any number of blocks to be used to cover an arbitrary three-dimensional region.[6] Any block can be linked to any other block, with complete continuity across the block interfaces. The composite structure is such that completely general configurations may be treated, the arrangement of the subregions being specified by input, without modification of the code. The code includes a three-dimensional algebraic generation system based on transfinite interpolation for the generation of an initial solution to start the iterative solution of the elliptic generation system. This feature also allows the code to be run as an algebraic generation system if desired.

This code uses an elliptic generation system with automatic evaluation of control functions from boundary point distributions. Several procedures for determining the control functions from the boundary point distributions are incorporated in the code, and it was the purpose of the present study to evaluate the effectiveness

[*] Lt, USAF, Computational Aerodynamicist, Member AIAA
[+] Professor, Aerospace Engineering, Member AIAA

of these procedures with regard to Euler solutions.

The elliptic grid generation system is defined by:

$$\sum_{m=1}^{3} \sum_{n=1}^{3} g^{mn} r_{\xi^m \xi^n} \cdot \sum_{n=1}^{3} g^{nn} P_n r_{\xi^n} = 0 \tag{1}$$

where the g^{mn} are the elements of the contravariant metric tensor:

$$g^{mn} = \nabla_\xi^m \cdot \nabla_\xi^n \tag{2}$$

These elements are more conveniently expressed in terms of the elements of the covariant metric tensor, g_{mn}:

$$g_{mn} = r_{\xi^m} \cdot r_{\xi^n} \tag{3}$$

which can be calculated directly. Thus

$$g^{mn} = \frac{1}{g}(g_{jk} g_{lj} - g_{jl} g_{jk}) \tag{4}$$

(m,i,j) cyclic, (n,k,l) cyclic,

where g, the square of the Jacobian, is given by

$$g = \det |g_{ij}| = r_{\xi^1} \cdot (r_{\xi^2} \times r_{\xi^3}) \tag{5}$$

In these relations, r is the Cartesian position vector of a grid point ($r = ix + jy + kz$), and the ξ^i ($i=1,2,3$) are the three transformed, curvilinear coordinates. The P_n are the "control functions" which serve to control the spacing and orientation of the grid lines in the field.

Negative values of the control function P_n cause grid lines on which ξ^n is constant to move in the direction of decreasing ξ^n. This feature can be used to concentrate grid lines near other grid lines and/or points or in certain regions of physical space. However, a more automatic procedure is to determine the control functions so as to project the boundary point spacing into the field. The details are discussed in reference 3; however, a brief explanation is presented here.

Consider first a rectangle with equally spaced points on the horizontal sides but unequal spacing on the two vertical sides (Fig. 1). With no control functions, i.e., $P_n=0$, Eq. (1) will produce a grid that attempts to be equally spaced in the interior of the region, (Fig. 2). A grid of parallel lines for this configuration, reflecting the unequal spacing on the boundaries (Fig. 3), can only be produced from Eq. (1) with $P_2 \neq 0$ (taking ξ^1 to vary on the horizontal sides and ξ^2 to vary on the vertical sides).

The proper values of P_2 needed to accomplish this are determined by evaluating Eq. (1) one-dimensionally on the vertical sides, with the result

$$y_{\xi^2 \xi^2} + P_2 \, y_{\xi^2} = 0$$

where:

$$y_{\xi^2 \xi^2} = g^{22} r_{\xi^2 \xi^2}$$

and

$$y_{\xi^2} = g^{22} r_{\xi^2}$$

so that

$$P_2 = -\frac{y_{\xi^2 \xi^2}}{y_{\xi^2}} \tag{6}$$

With the J points on the vertical sides, and I points on the horizontal sides, the control function P_2 on the vertical sides then can be evaluated (using a central difference technique for Eq. (6)) from the point distribution thereon as

$$P(1,j) = -\frac{[y(1,j+1) - 2y(1,j)+y(1,j-1)]}{\frac{1}{2}[y(1,j+1) - y(1,j-1)]}$$

for $j=2,3,--,J-1$, with an analogous equation with I for the first argument. The values of P_2 in the interior of the region then can be interpolated from values of P_2 on the two vertical sides. A similar evaluation of the other control function, P_1, on the two horizontal sides from

$$P_1 = -\frac{x_{\xi^1 \xi^1}}{x_{\xi^1}} \tag{7}$$

produces a zero in the present case due to equal spacing on these sides. In the case of unequal spacing, the values of P_1 in the interior of the region would be evaluated by interpolation between the values on the two horizontal sides. With the control functions evaluated in this manner, Eq. (1) will produce a grid composed of parallel straight lines for this boundary configuration, thus reflecting the boundary point spacing into the field (Fig. 3).

Now consider an O-type grid with two concentric circular boundaries and equally spaced points around the circles (Fig. 4). Because of its inherent tendency to cause the grid lines to move closer to convex boundaries, Eq. (1) with no control functions will produce a grid with unequal radial spacing of the circumferential lines (Fig. 5). In this case, evaluation of Eq. (1) with the polar coordinate transformation;

$$x(r,\theta) = r(\xi^2)\cos\theta$$
$$y(r,\theta) = r(\xi^2)\sin\theta$$

yields the equation

$$P_2 = -\frac{r_{\xi^2 \xi^2}}{r_{\xi^2}} + \frac{r_{\xi^2}}{r} \tag{8}$$

Thus, in order to produce a specified radial distribution of lines, the control function P_2 must be evaluated from Eq. (8) using the given distribution $r(\xi^2)$. First, a radial cut is made in the physical plane from the inner to the outer circle. The circular region can now be unwrapped to form a computational field that has its two vertical sides corresponding to the cut between the two circular boundaries in the physical field (Fig. 6). Therefore, with the specified radial distribution placed on the two vertical sides of the computational field, the control function P_2 can be evaluated from Eq. (8) on these sides as

2

$$P(i,j) = -\frac{[r(i,j+1)-2r(i,j)+r(i,j-1)]}{\frac{1}{2}[r(i,j+1)-r(i,j-1)]} \cdot$$

$$\frac{\frac{1}{2}[r(i,j+1)-r(i,j-1)]}{r(i,j)} \qquad (9)$$

and a similar equation with I as the first
argument. The interior values then can be
determined by interpolation between the two
vertical sides as before. Note that this amounts
to interpolation in the circumferential direction
in the physical plane. Again, equal spacing
around the circles produces a zero value of the
other control function, P_1. In general, P_1 would
be evaluated on the two circles and interpolated
between the two horizontal sides in the
computational region, i.e., between the two
circles in the physical field. Both the radial
and circumferential interpolation schemes are
represented in Figure 7.

The second term in Eq. (8) arises from the
curvature of the boundary, and the denominator is
the local radius of curvature of the grid line
that is to pass through the point where the
control function is being evaluated. This term
acts to reduce the magnitude of the control
function in order to allow for the natural
tendency of the grid lines to move toward convex
boundaries. Since the lines tend to concentrate
near the inner circle even with zero control
functions, the use of the first term alone in Eq.
(8), (in analogy with the flat boundary case,
i.e., Eq. (6)), would produce a stronger
concentration of lines near the inner circle than
was intended.

Finally, consider a C-type grid (Fig. 8), with
the resulting computational region (Fig. 9). If
now the control function P_2 is evaluated on lines
1-2 and 4-3 in the physical field from Eq. (6),
and the interior values are interpolated between
the two vertical sides in the computational field,
the resulting control function, while serving well
over the right portion of the physical field, will
be too strong over the inner body where the line
curvature is not zero. The use of Eq. (8) on the
lines 1-2 and 4-3 would be no better since the r
in the denominator is to be interpreted as the
local radius of curvature of the crossing line and
hence is infinite on these lines so that the
second term in Eq. (8) vanishes.

This situation can be remedied by
interpolating for the local radius of curvature in
Eq. (8) between the inner and outer boundaries in
the physical field, i.e., between the horizontal
sides in the computational region. However, since
the ξ^2 derivatives in Eq. (8) must still be
evaluated on the vertical sides it is necessary to
separate Eq. (8) into three pieces:

$$P_2 = \left(\frac{r_\xi^2 \xi^2}{r_\xi^2}\right) + \frac{(r_\xi^2)}{r} \qquad (10)$$

Now the two quantities in parentheses are
evaluated on the vertical sides of the
computational region, while the radius of
curvature is evaluated on the two horizontal
sides. The control function in the interior then

is evaluated by interpolating the quantities in
parentheses between the vertical sides,
interpolating the radius of curvature between the
horizontal sides, and then evaluating P_2 from Eq.
(10) using these interpolated values. Note that
this procedure supplies a finite radius of
curvature over the inner body, thus reducing the
control function appropriately in this region.

A problem arises, however, when the radius of
curvature (r) is of opposite sign on the two
boundaries between which it is interpolated (Fig.
10), since then the interpolation will produce a
zero value at some point in between, and at such a
point the second term of Eq. (10) is infinite.
This problem can be corrected by interpolating
1/r, instead of r. This amounts to writing Eq.
(10) as

$$P_2 = \left(\frac{-r_\xi^2 \xi^2}{r_\xi^2}\right) + (r_\xi^2)\,\frac{1}{r} \qquad (11)$$

and interpolating the curvature (1/r), rather than
the radius of curvature (r).

Although the exact equations for the general
case are more complicated, the control function,
P_n, may still consist of spacing terms along a
boundary and terms arising from the local
curvature of crossing lines. This amounts to
interpolating the spacing terms between the four
sides on which ξ^n varies (Fig. 11) and
interpolating the local curvature terms between
the two sides on which P_n is constant (Fig. 12).
The question that then arises is whether the
transfinite interpolation for the spacing term and
the local curvature term should use linear
blending functions or blending functions based on
physical arc length. The former (linear) amounts
to interpolating in terms of the transformed
curvilinear coordinate, while the latter (arc)
amounts to interpolation with respect to the
physical distance. For example, on the grid
illustrated in Fig. 13, interpolation with
"linear" blending functions would produce a value
on line 3 that is the average of that on lines 1
and 5, while with "arc" blending functions the
value produced on line 3 would be closer to this
on line 1.

Flow Solver

For this investigation a three-dimensional
time-dependent Euler approximation, developed by
Whitfield,[12] was employed using finite volume
discretization and a second-order implicit scheme
to solve the flux-vector-split form of the
equations with local time stepping. This scheme
solves 5x5 block bi-diagonal systems of equations
using Doolittle's method.[13] Characteristic
variable boundary conditions are used in the
farfield and at impermeable surfaces. No
additional artificial dissipation is added, and
the scheme is conditionally stable in three
dimensions. Optimum CFL numbers appear to be
between 12.5 to 15.

Configuration and Flow Conditions

Three generic weapon/store configurations are
examined using the various gridding procedures and
grid types. The first geometry (Configuration 1)

3

consists of a 10/3 D cylindrical centerbody and 5/3 D tangent ogive forebody and afterbody[14] (Fig. 14) and is modeled using an 81x15x10, O-type grid. This configuration is used to represent a typical fuel tank carried on current aircraft and is examined at two transonic Mach numbers, 0.85 and 1.20, both at zero degrees angle-of-attack. The second geometry (Configuration 2) consists of a 10° cone-cylinder[15] (Fig. 15) and is modeled using an 81x15x10, H-type grid. This geometry is used to represent a generic penetrator and is examined at $M_\infty=0.999$ and $\alpha=0^\circ$. The third geometry (Configuration 3) consists of a 1.5 D tangent ogive forebody and a 20 D cylindrical aft section[15] (Fig. 16) and is modeled by a 65x20x10, C-type grid. This configuration is used to model a high-fineness ratio (21.5:1) body-alone missile airframe, and is analyzed in the subsonic range at $M_\infty=0.70$ at $\alpha=5.07^\circ$ and in the transonic range at M $=0.90$ at $\alpha=0^\circ$.

Analysis

Two investigations examined control function interpolation techniques. The first analysis involved employing both the "linear" and "arc" techniques for interpolating the spacing term in the control function. The second study investigates the use of the "linear" and "arc" techniques with respect to the radius of curvature (r) and curvature (1/r) interpolations for the local curvature term in the control function.

Spacing Term

Figure 17 shows the effects of the interpolation for the spacing term using the "linear" and "arc" techniques for the C-type grid on Configuration 3. Using the "linear" interpolation (Fig. 17a), the grid lines better reflect the concentrated point distribution in the shoulder region of the body, thereby aligning the grid with the shock pattern that develops near that location. Figure 17b shows a close-up view of the grid near the shoulder region of the body. Using the "arc" interpolation, the grid lines are slanted far forward and hence, do not align themselves with the shock pattern (Figs. 17c,d). Figure 18a shows the effects these two grids have on the Euler solution. Figure 18b gives an expanded view of the shock region. For the "linear" grid, a typical second-order solution to the Euler equations at $M_\infty=0.90$ and $\alpha=0^\circ$ is obtained. One expects the computed shock strength to be slightly higher than the experimental data at the peak of the expansion and, although not desirable, second-order "ringing" (dispersive effects) is expected downwind of the shock for this upwind scheme. The "linear" grid solution shown has expanded at the shock more than one expects, but does reflect the characteristics of the inviscid solver. The "arc" grid solution, although more closely matching the experimental data, does not reflect the qualities of an accurate, second-order, inviscid solution. Figure 19 shows the effects these two grids have on the Euler solution at $M_\infty=0.70$ and $\alpha=5.07^\circ$. The "linear" grid solution, once again, reflects a typical second-order, inviscid solution by over predicting the expansion and, since no shock was formed, exhibits no dispersive effects (ringing). The "arc" grid solution shows similar results in

which the expansion is overpredicted and no dispersive effects are witnessed downwind of the expansion.

Although not shown, similar results are obtained for Configuration 1 (O-type grid) at both flow conditions and Configuration 2 (H-type grid) at $M_\infty=0.999$ and $\alpha=0^\circ$. These results again show that the "linear" interpolation technique for the spacing term reflects a more accurate second-order, inviscid solution for all cases.

Local Curvature Term

The first part of this analysis examines the effects of interpolating for the radius of curvature (r) using both the "linear" and "arc" techniques to obtain the local curvature term in the control function. Figure 20 shows the effects of these two techniques for the O-type grid on Configuration 1. Using the "arc" technique, a better concentration of grid lines is obtained close to the body (Fig. 20a,b). Using the "linear" technique, a comparable grid is produced; however, the grid is not as concentrated near the body (Fig. 20c,d). Figure 21 shows the effects these two grids have on the Euler solution at $M_\infty=1.20$ and $\alpha=0^\circ$. The "arc" grid, with its greater concentration of lines near the body, resolves the flowfield more accurately in the stagnation region. Physically reasonable results are obtained using the "arc" grid in which the first cell on the nose yields a higher pressure coefficient (C_p) than does the second or third cell (Fig. 21b). The "linear" grid yields unreasonable results in which the third cell back on the nose yields a higher C_p than does the first or second cell (Fig. 21b). Figure 22 shows the effects these two grids have on the Euler solution at $M_\infty=0.85$ and $\alpha=0^\circ$. Both grids yield physically reasonable, although markedly different, results at these flow conditions.

Similar results are obtained for Configuration 2 at $M_\infty=0.999$ and $\alpha=0^\circ$ and for Configuration 3 at both flow conditions. These results show that interpolating for the radius of curvature (r) using the "arc" technique to obtain the curvature term in the control function yields a more physically reasonable solution for all cases.

Due to the fact that complications can arise when interpolating for the radius of curvature (r), a second examination is performed to study the effects of interpolating for the curvature (1/r) using both the "linear" and "arc" techniques. Figure 23 shows the effects of using the "arc" technique on the O-type and C-type grids. This technique yields an undesirable grid in which the lines are highly skewed and, hence, is not useful to the Euler solver. Therefore, when interpolating for the curvature (1/r) only the "linear" technique should be used.

Control Function

Depending on the geometry, there are two optimum approaches for obtaining the control function, P_n. The first method is to employ the "linear" technique to obtain the spacing term and, when the two opposing boundaries have curvature of the same sign, to interpolate for the radius of

curvature (r) using the "arc" technique to obtain the local curvature term (Method 1). The second method is to, again, employ the "linear" technique to obtain the spacing term and, when the two opposing boundaries have curvature of the opposite sign, to interpolate for the curvature using the "linear" technique to obtain the local curvature term (Method 2).

These two methods yield similar grids and a thorough comparison shows that both methods give approximately the same Euler solutions. Figure 24 shows the effects of these two methods on Configuration 1 (O-type grid) at $M_\infty = 1.20$ and $\alpha = 0°$. The results are essentially the same except in the stagnation region where Method 2 (spacing: "linear", local curvature: curvature - "linear") does not concentrate the grid lines as close to the body and; hence, does not appropriately resolve the flowfield (Fig. 24b). Figure 25 shows the effects of these two methods on Configuration 2 (H-type grid) at $M_\infty = 0.999$ at $\alpha = 0°$. These results show that both methods yield essentially identical solutions. Figure 26 shows the effects of these two methods on Configuration 3 (C-type grid) at $M_\infty = 0.90$ and $\alpha = 0°$. Again, these results show that both methods yield the same second-order, inviscid solution.

As can be seen by a comparison of Figures 20 and 23 and the results in Figure 24, it is advisable to interpolate for the radius of curvature (r), rather than the curvature (1/r), to obtain the local curvature term in the control function when the curvature has the same sign on the two opposing boundaries. In fact, interpolating for the curvature (1/r) does not produce the exact form given by Eq. (8) for the simple case of two concentric circles.

Conclusions and Recommendations

This study has demonstrated the viability of automatic determination of the control function from the boundary point distributions using separate interpolation of the terms arising from spacing and those arising from local curvature. The following is recommended as the optimum approach for obtaining the control function in the elliptic grid generation system (Eq. 1). For the spacing term, the "linear" blending approach should be employed globally. For the local curvature term, global interpolation for the radius of curvature (r) using the "arc" technique should be employed. However, when the two opposing boundaries have curvature of the opposite sign, local interpolation for the curvature (1/r) using the "linear" technique should be used.

It has been shown throughout this analysis that various grid generation techniques employed within the code do have a substantial impact on the solution and, when care is taken to generate the grid in the proper manner, these grids help the flow solver to yield accurate second-order, inviscid solutions.

References

[1]Shin, T.I-P., Finite Difference Methods in Computational Fluid Dynamics, to be published by Prentice-Hall Co.

[2]Kutler, P., "A Perspective of Theoretical and Applied Computational Fluid Dynamics," AIAA Paper 83-0037, Reno, Nev., Jan. 1983.

[3]Thompson, J.F., Warsi, Z.U.A. and Mastin C.W., Numerical Grid Generation: Foundations and Applications: North-Holland 1985.

[4]Thompson, J.F., "A Survey of Grid Generation Techniques in Computational Fluid Dynamics," AIAA Paper 83-0447, Reno, Nev., Jan. 1983.

[5]Thompson, J.F., "A Survey of Dynamically-Adaptive Grids in the Numerical Solution of Partial Differential Equations," Applied Numerical Mathematics, pp. 3-27, 1985.

[6]Thompson, J.F., "A Survey of Composite Grid Generation for General Three-Dimensional Regions," to appear in Numerical Methods for Engine Airframe Integration, S.N.B. Murthy and G.C. Payntor (ed.), AIAA.

[7]Eiseman, P.R., "Grid Generation for Fluid Mechanics Computations, Annual Review of Fluid Mechanics, Vol 17, 1985.

[8]Thompson, J.F. (Ed.), Numerical Grid Generation, North-Holland, 1982. (Also published as Vol. 10 and 11 of Applied Mathematics and Computation, 1982).

[9]Smith, R.E. (Ed.), Numerical Grid Generation Techniques, NASA Conference Publication 2166, NASA Langley Research Center, 1980.

[10]Ghia, K.N., and Ghia, U. (Ed.), Advances in Grid Generation, FED-Vol. 5, ASME, Applied Mechanics, Bioengineering, and Fluids Engineering Conference, Houston, 1983.

[11]Kaul, U., and Chaussee, D.S., "A Comparative Study of Parabolized Navier-Stokes (PNS) Code Using Various Grid Generation Techniques," AIAA Paper 84-0459, Reno, Nev., Jan. 1984.

[12]Whitfield, D.L., "Implicit Upwind Finite Volume Scheme for the Three-Dimensional Euler Equations," Mississippi State University Paper EIRS-ASE-85-1, Sept. 1985.

[13]Dahlquist, G. and Bjorck, A., Numerical Methods Prentice-Hall, Inc., Englewood Cliffs, N.J., 1974.

[14]Mrdeza, M.N., "CFD Unfinned Store Mutual Interference Wind Tunnel Experiment," AEDC-TSR-85-P21, Calspan Corp./AEDC Division, Nov. 1985.

[15]Hartman, K., "1.5 D Ogive-Circular Cylinder Body, L/D-21.5," Experimental Data Base for Computer Program Assessment, AGARD Paper AR-138, May 1979.
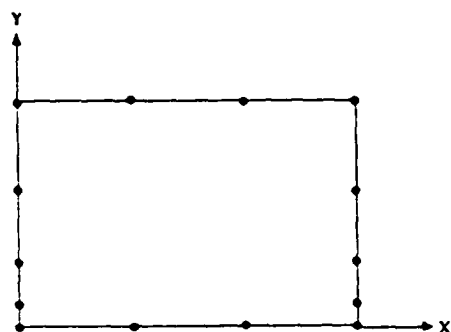
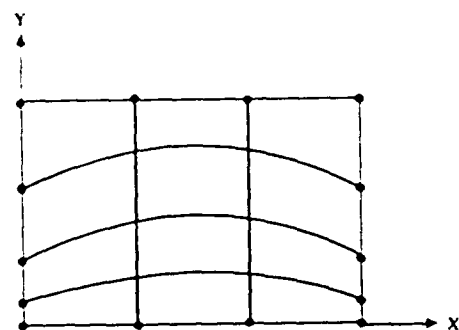Figure 1. Unequal Spacing on Vertical Sides

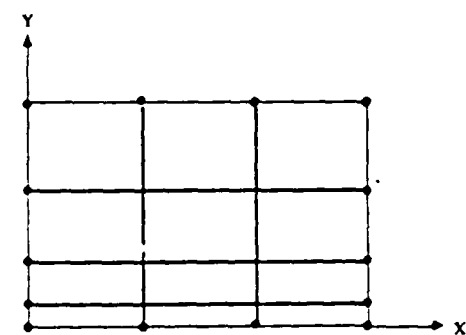Figure 2. Equally Spaced Lines in Interior of Grid
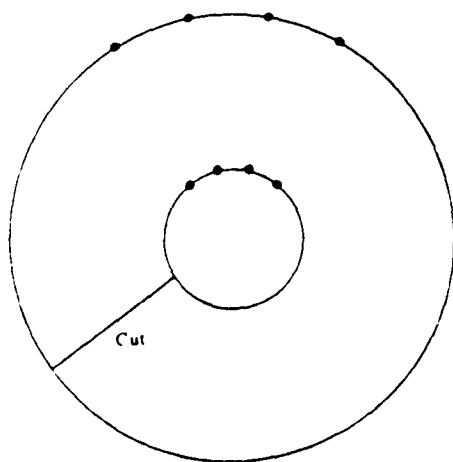
Figure 3. Grid of Parallel Lines

Figure 4. Equally Spaced Points Around Circles

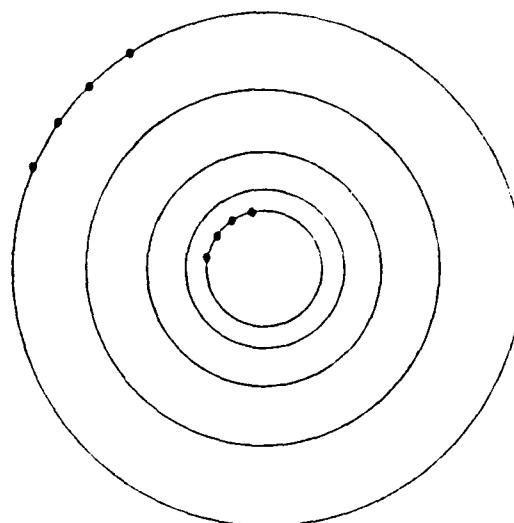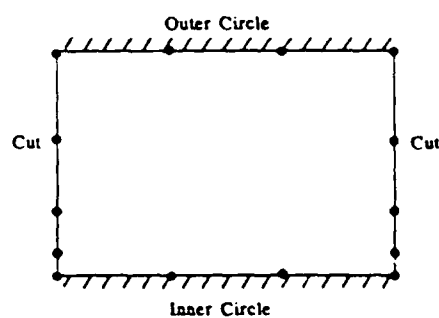Figure 5. Unequal Radial Spacing of Circumferential Lines
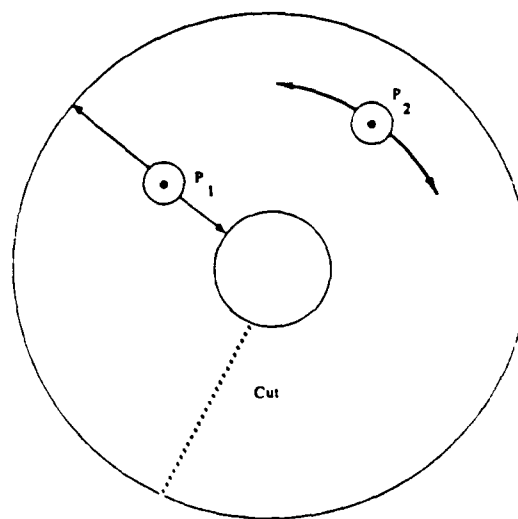
Figure 6. Computational Region

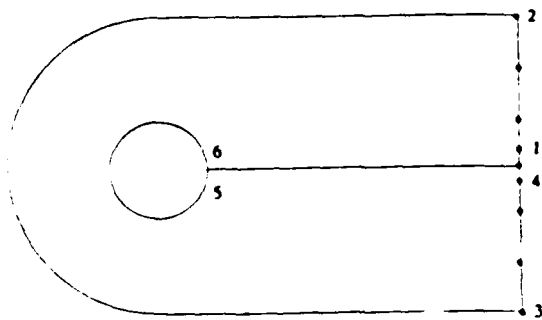Figure 7. Radial (P_1) and Circumferential (P_2) Interpolation Schemes
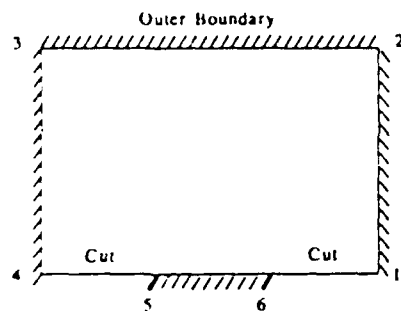
6

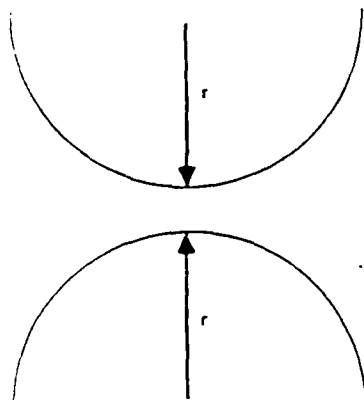Figure 8. C–Type Grid, Physical Region

Figure 9. Computational Region
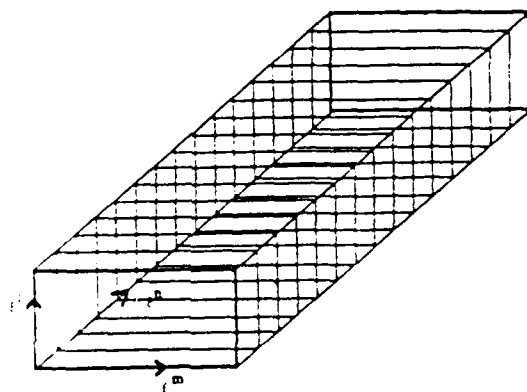

Figure 10. Radius of Curvature (r) With Opposite Signs

Figure 11. Four Sides on Which ξ^n Varies
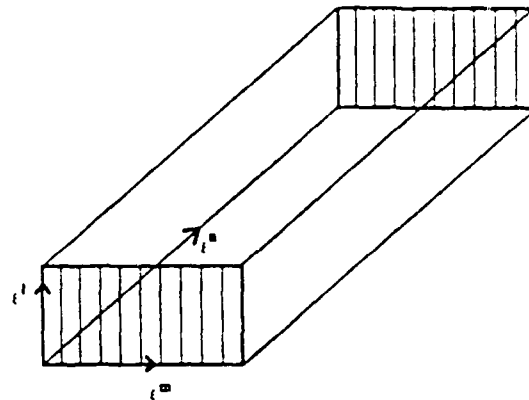
Figure 12. Two Sides on Which P_n is Constant
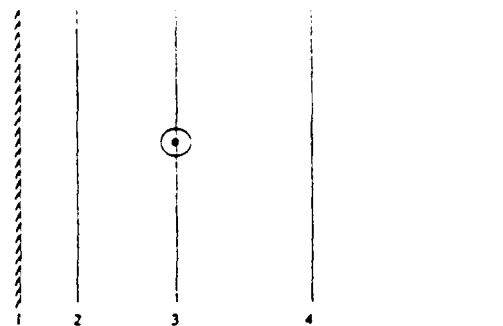
Figure 13. Interpolation Techniques
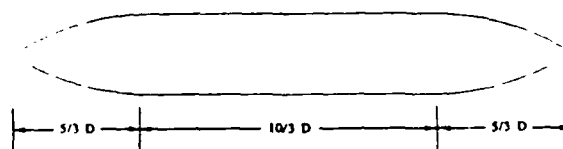
Figure 14. Configuration 1
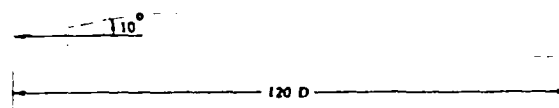
Figure 15. Configuration 2
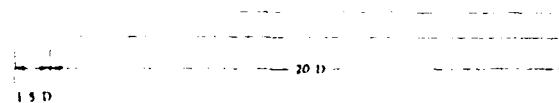
Figure 16. Configuration 3

7

Figure 17a. "Linear" Interpolation for
Spacing Term (C-Type)
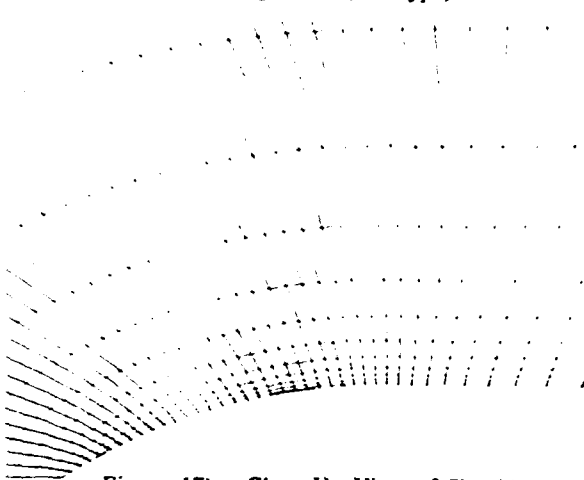
Figure 17b. Close Up View of Shoulder
Region ("Linear")
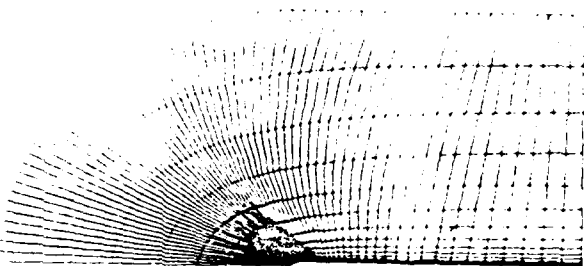
Figure 17c. "Arc" Interpolation of
Spacing Term (C-Type)
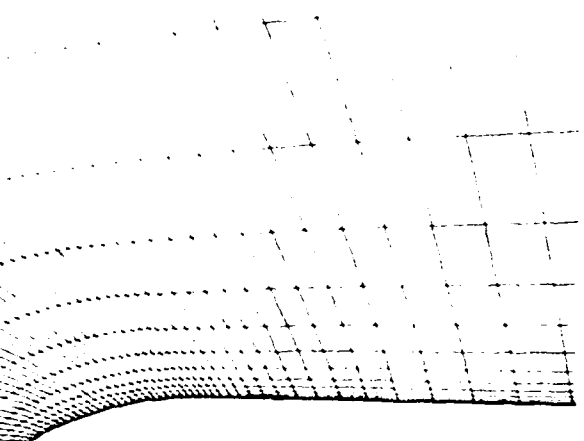
Figure 17d. Close Up View of Shoulder
Region ("Arc")

Figure 18a. Surface Pressure Distribution
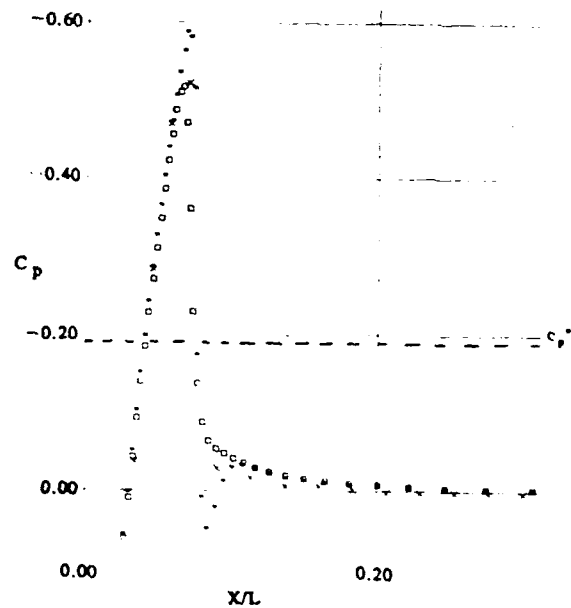
Figure 18b. Expanded View of Shock Region

8
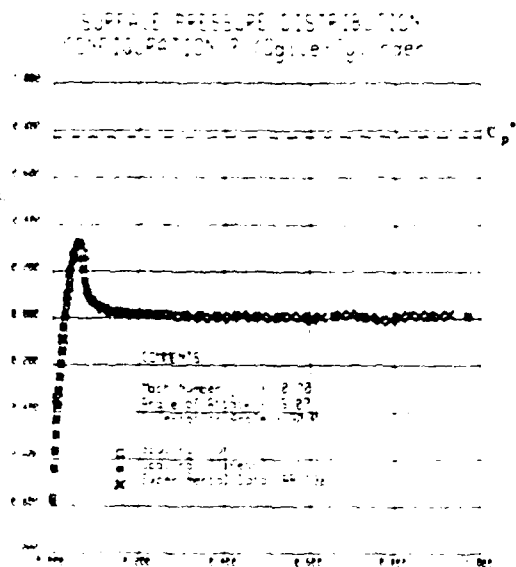
Figure 19. Surface Pressure Distribution

Figure 20c. "Linear" Interpolation of Local
Curvature Term (O-Type)
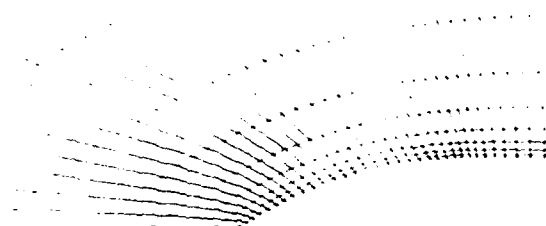
Figure 20d. Close-Up View of Stagnation
Region ("Linear")

Figure 20a. "Arc" Interpolation for Local
Curvature Term (O-Type)

SURFACE PRESSURE DISTRIBUTION
CONFIGURATION 1 (Ogive-Cylinder-Ogive)

Figure 20b. Close Up View of Stagnation
Region ("Arc")
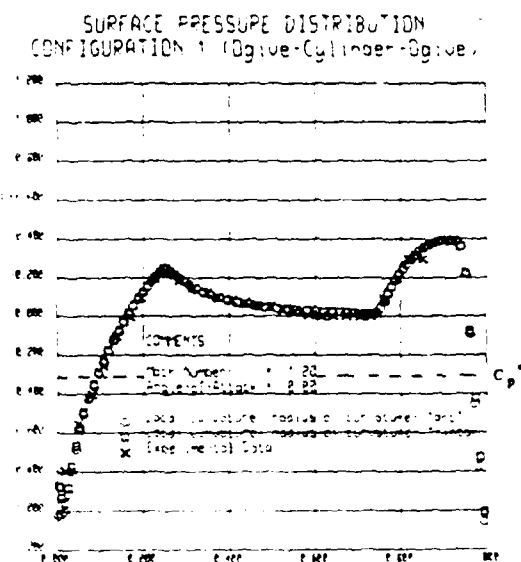
Figure 21a. Surface Pressure Distribution

9

Figure 23a. Curvature Interpolation Using "Arc" Technique (O–Type)

Figure 21b. Expanded View of Stagnation Region
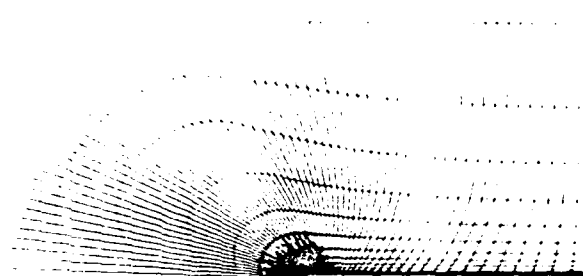
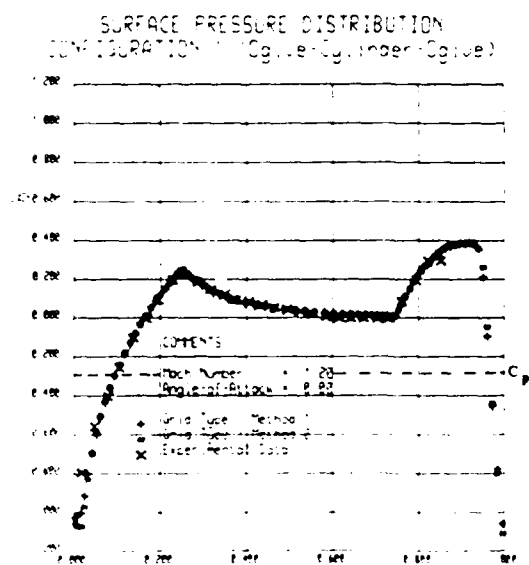Figure 23b. Curvature Interpolation Using "Arc" Technique (C–Type)
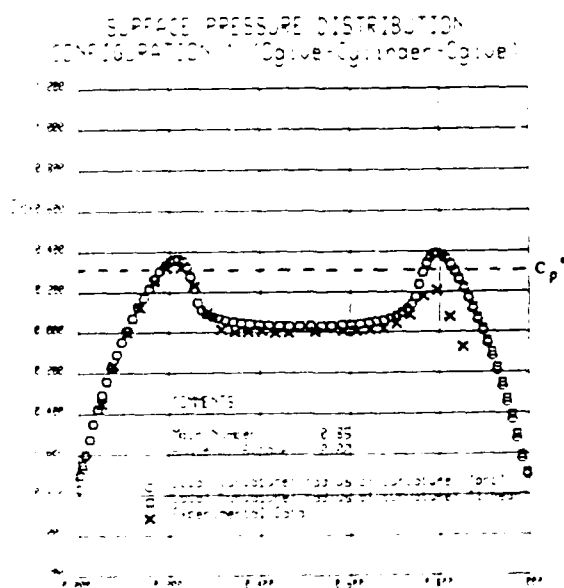
Figure 22. Surface Pressure Distribution

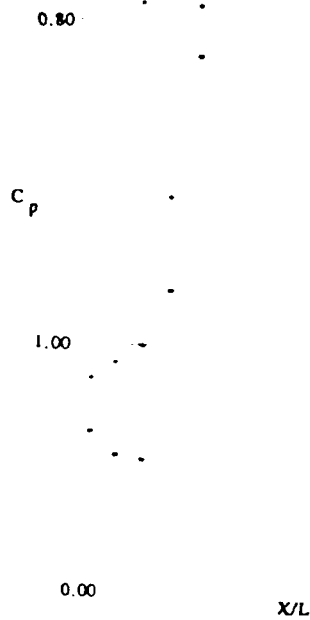
Figure 24a. Surface Pressure Distribution

0.80

C_p

1.00

0.00

X/L

Figure 24b. Expanded View of Stagnation Region

SURFACE PRESSURE DISTRIBUTION
CONFIGURATION 3 (Ogive-Cylinder)

X/L

Figure 26. Surface Pressure Distribution

SURFACE PRESSURE DISTRIBUTION
CONFIGURATION 2 (Cone-Cylinder)
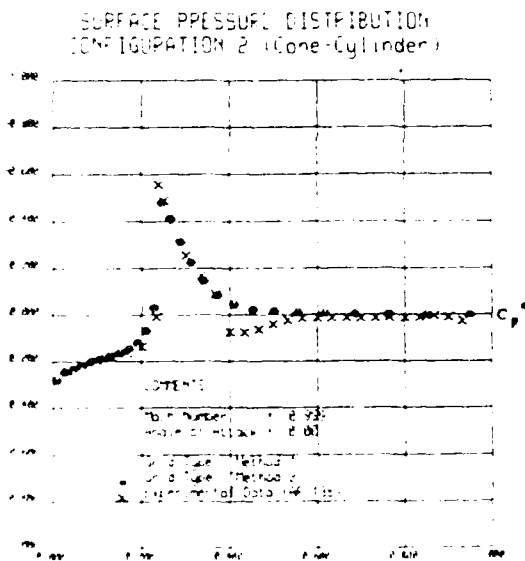
Figure 25. Surface Pressure Distribution

11

END

DTIC

7 – 86